Applied Mathematics & Information Sciences
An International Journal

http://dx.doi.org/10.18576/amis/190407

Optimizing Histopathological Imaging Analysis for Breast Cancer Detection using Enhanced Pelican Optimization Algorithm and Deep Feature Fusion

Arwa Darwish Alzughaibi[1], *Maryam Alsolami*[2], *Mohammed Alshahrani*[3,*], *Sultan Ahmed Almalki*[3], *Mohammed Al-Jabbar*[3], *and Randa Alharbi* [4]

[1] Applied College, Taibah University, Medina, Saudi Arabia
[2] Department of Computer Science and Artificial Intelligence, College of Computing, Umm Al-Qura University, Makkah, Saudi Arabia
[3] Computer Department, Applied College, Najran University, Najran 61441, Saudi Arabia
[4] Department of Statistics, Faculty of Science, University of Tabuk, Tabuk, Saudi Arabia

Received: 5 Dec. 2024, Revised: 15 Feb. 2025, Accepted: 11 Mar. 2025
Published online: 1 Jul. 2025

Abstract: Breast cancer (BC) is a major common type of cancer in women. Earlier and accurate diagnoses of BC may enhance the treatment chances and reduce the mortality rate. Therefore, the emergence of reliable and accurate Computer-Aided Diagnosis (CAD) system BC images is a pressing concern for earlier diagnoses. Classical algorithms limit pathologists' skills and are time-consuming. Automated histopathological image (HI) classification is an area of interest that might reduce the risk of mistakes and speed up BC diagnoses. Histopathology uses a biopsy to capture images of the diseased tissue. Lately, deep learning (DL) techniques have shown great efficiency in different medical imaging applications, such as the processing of HI. Therefore, this article develops an automated Histopathological Imaging Analysis for BC Detection using the Enhanced Pelican Optimization Algorithm and Deep Feature Fusion (BCD-EPOADFF) technique. The purpose of the BCD-EPOADFF technique is to examine the histopathological images for the detection and classification of BC. In the BCD-EPOADFF technique, the adaptive median filtering (AMF) technique can be applied to get rid of the noise and enhance the image quality. In the BCD-EPOADFF technique, a deep feature fusion process takes place comprising three DL models namely Residual Networks (ResNet), EfficientNet, and InceptionNet. Moreover, the hyperparameter tuning of the DL models takes place using EPOA which incorporates the traditional POA with oppositional-based learning (OBL) concept. Finally, the fuzzy neural network (FNN) model can be employed for automated detection and classification of BC. To validate the enriched performance of the BCD-EPOADFF method, wide-ranging simulations were involved. The experimental results stated the superior performance of the BCD-EPOADFF method over other models for distinct measures.

Keywords: Breast Cancer; Histopathological Image; Computer-Aided Diagnosis; Feature Fusion; Pelican Optimization Algorithm

1 Introduction

Cancer is a major public health issue around the world. Particularly, Breast cancer (BC) is the most prevalent cancer in women [1]. In the 1970s, the number of BC patients improved across the world, and till now, BC has become the major cancer type with the maximum occurrence and mortality rates globally. As stated by information from the World Health Organization (WHO), 8.8 million population died in 2020 to be around 684,996. A histopathological analysis of BC is the "gold standard" for diagnosing BC. Pathologists can differentiate between non-malignant (benign) tissue, malignant cancer, and normal tissue by microscopically noticing its structure and collection of biopsy samples in histopathological images (HI) [2]. By comparison with conventional pathology, digital pathology employs digital pathological techniques for digitizing and network processing of pathological resources. In the medical sector, we can define the synchronous browsing of data, long-lasting storage, and collected visualization through the application of big data technology [3]. The process of gathering pathological resources will not be prolonged constraint by space and time. As a result, digital

* Corresponding author e-mail: moaalshahrani@nu.edu.sa

pathology has become extensively utilized in relevant domains of pathology [4].

Recently, factors of image analysis methods are comprised such as a huge rise in existing processing power, low-cost storage devices, and considerable development, which is facilitated by conventional computer-aided design (CAD) techniques in the day-by-day routine of pathology laboratories [5]. For disease identification, prognosis, and analysis, these technologies are established to enhance the decisions of pathologists or human experts. The automatic analysis of biomedical information offered by this advanced CAD technique will be support to the pathologist for achieving an earlier or timely diagnosis [6]. There will be a continuous requirement for CAD models or systems for minimizing the difficulty of pathologists by separating and filtering out the noticeable benign regions, supporting earlier recognition of BC, and reducing the mortality rates related to the disease [7]. Current advances in artificial intelligence (AI) and deep learning (DL) have proven significant outcomes for various applications, mainly in the domain of medicine and speech [8]. Especially, they have achieved an extensive development in the accurate identification of malignancies and rare diseases namely skin cancers, diabetic retinal (DR) detachment, pneumonia caused by viruses, and congenital cataracts, which are shown human expert-level accuracy in disease classification. The integration of DL and CAD provides the major potential for the earlier recognition of cancer as it is leveraging big data in medical imaging and improving the effectiveness of widespread CAD systems [9]. Currently, the HI analysis employing DL methods will attained considerable attention because of its capability for improved analyzing cancer and enriching cancer research. Histopathology includes the microscopic analysis of tissue samples for identifying abnormalities like cancerous cells and other diseases [10]. DL techniques provide a robust toolset for automating and increasing this method.

This article develops an automated Histopathological Imaging Analysis for BC Detection using the Enhanced Pelican Optimization Algorithm and Deep Feature Fusion (BCD-EPOADFF) technique. In the BCD-EPOADFF technique, adaptive median filtering (AMF) technique can be applied to get rid of the noise and improve the image quality. In the BCD-EPOADFF technique, a deep feature fusion process takes place comprising three DL models namely Residual Networks (ResNet), EfficientNet, and InceptionNet. Moreover, the hyperparameter tuning of the DL models takes place using EPOA which incorporates the traditional POA with oppositional-based learning (OBL) concept. Finally, the fuzzy neural network (FNN) model can be applied for automated detection and classification of BC. The experimental results stated the superior performance of the BCD-EPOADFF method over other models in terms of distinct measures.

2 Literature works

Obayya et al. [11] introduced an arithmetic optimizer algorithm with a DL-based histopathological BC classification (AOADL-HBCC) method. This system utilizes noise removal dependent upon contrast improvement and median filtering (MF) technique. Moreover, an AOA with a SqueezeNet architecture to develop feature vectors was also implemented. Then, a deep belief network (DBN) model with an Adamax optimizer was employed for categorization. In [12], an innovative patch-based DL technique named Pa-DBN-BC was designed to detect and classify BC under HI employing the DBN. Features have been mined over the supervised fine-tuning stage and unsupervised pretraining. Automatically, the network could be extracted features in image patches. Logistic regression (LR) has been implemented for categorizing the patches at the HI. Chattopadhyay et al. [13] projected an innovative end-wise DL method called Multi-scale Dual Residual Recurrent Network (MTRRE-Net) for categorizing the BC from HI. The developed technique presents a contrasting method of dual residual block integrated with the RNN to address the vanishing gradient issue while the network must be considerably strong.

Sampath and Srinath [14] implemented an innovative method named a “Hybrid CNN” incorporating the transfer learning (TL) with the Sine Cosine Algorithm (SCA) model. The method employs a TL method, and the determined hyperparameters through SCA were utilized in the VGG 16 model. ImageNet should be applied for pretraining the network and the ultimate three convolution layers should be trained to employ TL. In [15], an innovative and robust technique dependent upon the convolutional-LSTM (CLSTM) learning algorithm, and the enhanced SVM method has been developed. The classification could be considerably increased by utilizing the process of HIs along with MWSA. For eight-class and binary classification methods, the greatest scores have been achieved through the improved SVM algorithm with the Bayesian optimization (BO) model. Hameed et al. [16] proposed a DL technique for automatically classifying hematoxylin-eosin (H&E) stained BC-HI into benign tissue, healthy tissue, invasive carcinoma, and in situ carcinoma. The developed method utilized 6 middle layers of the Xception network for recovering intellectual and strong features from input images. This method improved the developed system under the original (unnormalized) database through 5-fold cross-validation.

In [17], a DL technique, BC Recurrence Network (BCR-Net) was designed that automatically forecasts ODX recurrence problems in the HI. The developed model can be a two phases. Primarily, it wisely samples differentiates features from whole-slide HI of BC patients. Secondarily, it automatically weights every feature over a numerous instance learning method for predicting the repetition score at the image level. Yang

and Guan [18] developed and examined an increased network architecture DenseNet-201-MSD for accomplishing the classification process of medical HI of BC. Initially, the image was pre-processed, and the conventional pooling layer was changed by several scaling decompositions to avoid overfitting because of the huge size of the image database. Then, the BN method was included before the activation function Softmax and Adam could be utilized for the optimization.

3 The Proposed Method

In this article, we have designed an automated Histopathological Imaging Analysis for the BCD-EPOADFF technique. The purpose of the BCD-EPOADFF technique is to examine the HI for identifying and classifying BC. The BCD-EPOADFF technique comprises AMF-based preprocessing, feature fusion model, POA-based hyperparameter tuning, and FNN-based classification process. Fig. 1 represents the overall flow of the BCD-EPOADFF technique.

3.1 Preprocessing

Initially, the AMF technique can be applied to get rid of the noise and enhance the image quality. Compared to the classical median filter (MF), the AMF is widely used as a de-noising technique [19]. The AMF is used to perform spatial processing to define which pixel in MRIs has been affected by noise. By comparing all the pixels in the MRIs, it categorizes pixels as noise to their neighboring pixels. The size of the neighborhood window will be adaptable. A pixel that is not architecturally aligned with a pixel is similar and dissimilar from the majority of its neighbors, is labelled as a noisy pixel. Next, this noisy pixel is exchanged by the median pixel value that distributes the noise labelling test. AMF modifies the size of the neighborhood window. However, the neighborhood window has been a constant over the filtering operation in classical MF. The AMF retains details of MR images viz., smooth non-impulsive noise and edges, however, the conventional MF does not perform well. As well, the AMF performs well on those noises, however, the standard MF does not while the impulse noise density will be higher.

Here, the AMF acts on a rectangular area S_{xy}. The AMF modifies the size of S_xy through the operation based on certain conditions. The AMF performs in two levels represented Level A and B.

Level l: $L_{11} = Z_{med} - Z_{\min}$

$L_{12} = Z_{med} - Z_{\max}$

If $L_{11} > 0$ AND $L_{12} < 0$, Go to level2

Otherwise, improve the window dimension.

If the window size $S \leq S_{\max}$, repeat level l.

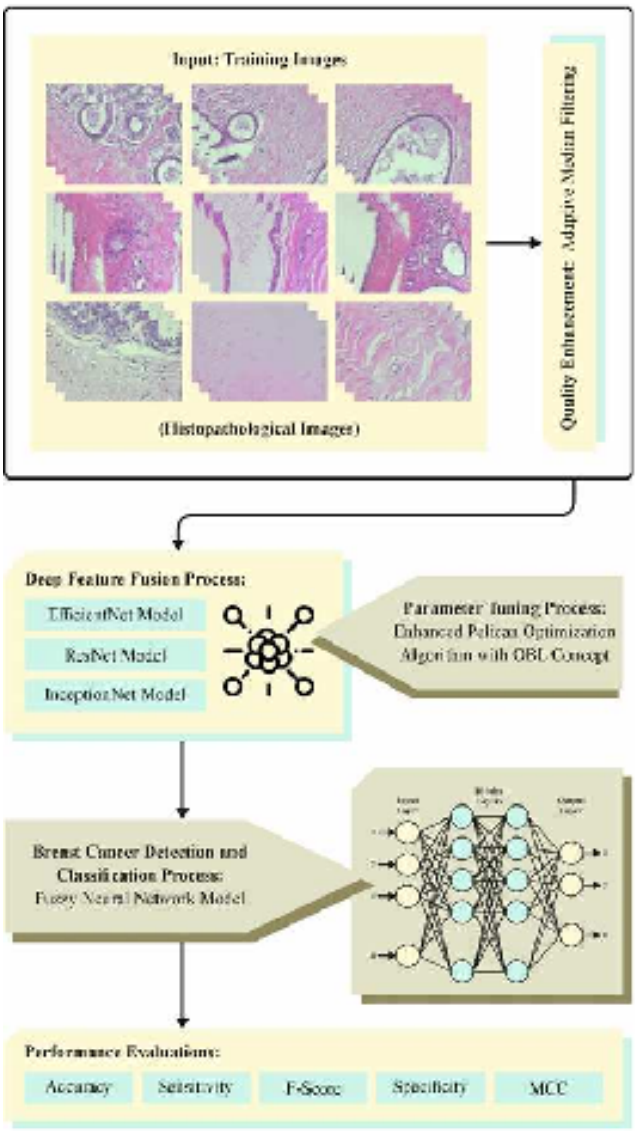

Fig. 1: Overall flow of the BCD-EPOADFF technique

Else output Z_{xy}.

Level2: $L_{21} = Z_{xy} - Z_{\min}$

$L_{22} = Z_{xy} - Z_{\min}$

If $L_{21} > 0$ And $L_{22} < 0$ output Z_{xy}

Else output Z_{med}.

Where $Z_{\max}$ and $Z_{\min}$ are the maximum and smallest gray level values in S_{xy}. Z_{med} is a median of the gray level in S_{xy}. $S_{\max}$ represents the maximum allowable size of S_{xy}.Z_{xy} refers to a gray level at (x, y) coordinates.

The filtering output is one value that exchanges the value of degraded pixel MR images at (x, y), at which point the S_{xy} is centered at the time.

3.2 Fusion-based Feature Extraction

In the BCD-EPOADFF technique, a deep feature fusion process takes place comprising three DL models namely ResNet, EfficientNet, and InceptionNet.

3.2.1 ResNet model

ResNet architecture is used to resolve the problems while training deep neural networks (DNN) [20]. Prior CNN often faces the problem of vanishing gradients once the massive amount of layers are stacked into NN. Gradient disappearing occurs once the network is deeper, and the gradient computed from the loss function reduces to zero using chain rule operation. As there is no weight updating, then the model has not learned anything from the training process.

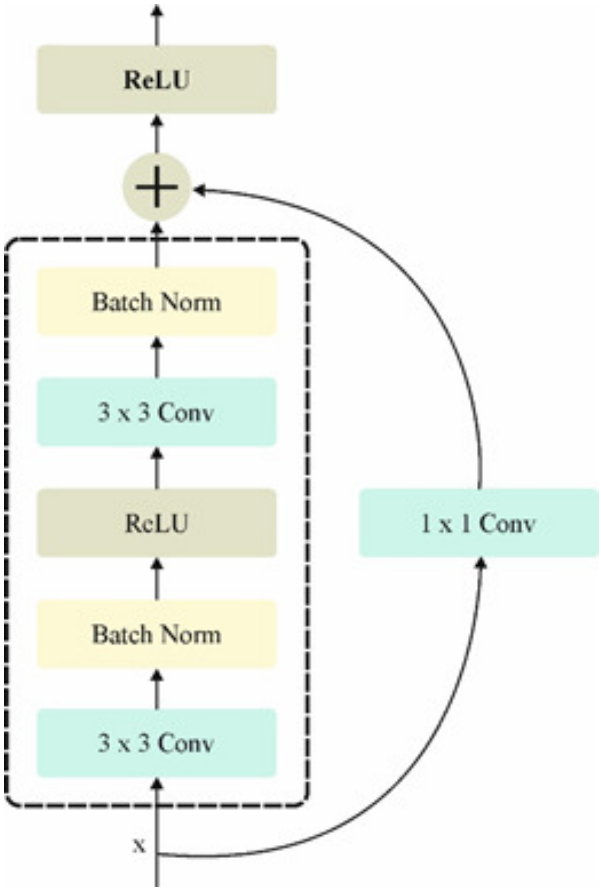

Fig. 2: Structure of ResNet

The principal idea of ResNet is the skip connection mode that decreases the vanishing gradient in two different ways. Firstly, a shortcut is established for the gradient passed over several layers that assist to be passed through several layers. Next, it enables us to learn an identity function that ensures high layers don't perform worse than the lower. As a variant of ResNet, ResNet50 includes 1 average pool layer, 1 max-pooling, and 48 convolution layers. Fig. 2 illustrates the infrastructure of the ResNet model.

ResNet adopts a residual learning model, we have x and y are the input and output of theth layer, and consider the building block:

$$y = F(x,\{W_i\}) + x \tag{1}$$

Where $F + x$ shows the shortcut or skip connection elementwise and operation function $F(x,\{W_i\})$ denotes the residual mapping to be learned.

3.2.2 EfficientNet model

Mixing Tan and Quoc Le, proposed EfficientNet and the researchers studied the relationships between the wide and the depth of the model compared to the network performance. A new type of model that has better classification performance and fewer parameters to scale on depth, wide, and resolution of input image is known as EfficientNet ranging from BO to B7 and passed each prior model on the classification task of ImageNet. The major component of EfficientNet is the MBConv (Mobile ConvNet) which has its origin in the MobileNet model. The EfficientNet model still performs a better classification accuracy compared to other CNNs like the EfficientNet BO with 5 million parameters and ResNet50 with around 20 million parameters.

The major role of EfficientNet is the new compound scaling model which consistently scales the resolution, depth, and width of the input image. This model can be mathematically expressed in the following:

$$\begin{cases} depth : d = \alpha^{\Phi} \\ width : w = \beta^{\Phi}, \quad s.T.\alpha.\beta^{\Phi}.\alpha^{\Phi}.\gamma^{\Phi} \approx 2, \alpha \geq 1, \beta \geq 1, \gamma \geq 1 \\ resolution : r = \gamma^{\Phi} \end{cases} \tag{2}$$

Where α, β, γ are constant coefficients measured by the smaller grid searching under the original lowest model. Φ denotes the coefficient predetermined by the users that control resources for the scaling model. We get 2^N times more computing resources if we scale the network width β^N, depth α^N, and resolution γ^N.

3.2.3 InceptionNet model

Before Inception Net, CNN focuses mainly on improving the depth for extracting features to enhance the learning capability. On the other hand, the creator of InceptionNet

established the scaling of the width and depth of the model while retaining continuous use of hardware. The fundamental concept behind the InceptionNet architecture is that all the neurons that extract similar features should learn together. Moreover, the InceptionNet model focuses on extracting different feature maps and parallel processing. A major aspect that makes InceptionNet unique from other CNNs before it. Also, the InceptionNet model has certain drawbacks, for instance, the large model that uses InceptionNet is subjected to overfit, particularly with a smaller amount of labelling input dataset. This will bias towards the class labels when compared to others.

3.3 POA-based hyperparameter tuning

The hyperparameter tuning of the DL methods takes place using EPOA which incorporates the traditional POA with OBL concept. The pelican is a massive bird with a long mouth and a huge weight in its throat to hold and consume the prey [21]. This kind of bird enjoys to live in groups of many pelicans. The appearance of pelicans is they generally have weight of 2.75 to 15 kg and 1.07 to 1.82 m in height. This type of bird usually takes fish, frogs, crustaceans, and turtles. If they are very hungry, they eat shrimp also. Pelicans often search in clusters and fall to their target from an elevation of 1020 meters after identifying its position. Few types search their target at the lowest heights also. After targeting, it spreads its wings under the surface of the water to pressure the prey into low water and then catches its target. If it grasps a fish, an extensive level of water enters its mouth, initiating pushing forward the fish and eliminating the additional water. Pelicans' behavior of searching and system will be a sophisticated tactic that has twisted these birds into superb hunters.

To upgrade solutions of the candidate, the developed POA imitates pelican behavior and approach when violent and searching target. At dual stages, this hunting model has been pretended:

1. Moving near prey (exploration stage).
2. Flying under the water surface (exploitation phase).

Moving near prey (Phase 1)

In the preliminary phase, the pelicans find their target and travel to that location. The exploration phase of the projected POA in finding various fields of search space has been improved by demonstrating this technique. The vital feature of POA becomes the target's place in the search space will be formed randomly. Exploration capability of POAs in the exact hunt of solving a problem space is enlarged as a solution for this. The previous ideas and Pelican's tactic for managing the target are arithmetically signified in Eq. (3).

$$x_{i,j}^{p_1} = \begin{cases} x_{i,j} + \text{rand}(p_j - I \cdot x_{i,j}), & F_p < F_i \\ x_{i,j} + \text{rand}(x_{i,j} - p_j), & \text{otherwise} \end{cases} \tag{3}$$

Where $x_{i,j}^{p_1}$ denotes the i^{th} pelican's novel grade in the j^{th} dimension, I refer to the random which is equivalent to either 1 or 2, p_j designates the prey position in the j^{th} dimension, and F_p denotes its goal function. I signify a number that may be either one or two randomly. This parameter is selected at random for every member and iteration. If this value of parameters is equal to 2, a member undergoes better movement, which outcome in the newest positions. As an outcome, parameter I affects the POA's capability to exactly survey the search space. This location has been recognized in the developed POA once the operation value is enhanced in that place. The method has been ended at migration near non-optimal locations in this kind of upgrading is recognized as an effectual update. Eq. (4) is utilized to perfect this procedure.

$$X_i = \begin{cases} x_{i,}^{p_1}, & F_i^{p_1} < F_i; \\ X_i, & else, \end{cases} \tag{4}$$

Where $F_i^{p_1}$ is assumed on phase 1 value of the objective function and $x_{i,}^{p_1}$ denotes the i^{th} pelican's novel status.

Flying on the water surface (Phase 2)

After getting to the surface of the water, pelicans used to enlarge their wings to raise the fish upper, and then collect the grasp in the throat. They are normally used to catch more extra fishes in the infected area as an outcome of this method. The projected POA meets at superior locations in the hunting area after exhibiting the behaviour of pelican. This method enhances POA's local search and exploitation abilities. To achieve an enhanced outcome, the algorithm must examine the opinions towards the pelican's position mathematically. Eq. (5) mathematically pretends the pelican's behaviour during hunting.

$$x_{i,j}^{p_2} = x_{i,j} + R\left(1 - \frac{t}{T}\right)(2 \cdot \text{rand} - 1)\, x_{i,j} \tag{5}$$

Where R denotes constant that was equal to 0.2, $x_{i,j}^{p_2}$ represents i^th pelican's novel grade in the j^{th} dimension, $R\left(1 - \frac{t}{T}\right)$ suggests the neighborhood range of $x_{i,j}$, t denotes the iteration count, and T refers to the highest iteration count. The "$R\left(1 - \frac{t}{T}\right)$" coefficient indicates the range of the population members' neighborhood to discover nearby every member to determine the finest

result. This coefficient has an outcome on the exploitation to become closer to the ideal global result. The coefficient value is important in the initial rounds, so a wider region over every member should be examined. The $\bullet(1-\frac{t}{T})$ " coefficient falls as the technique repeats, foremost in reduced ranges of every member's neighborhood. This enables us to scan the area over every population member in lesser, more exact stages, allowing the algorithm to converge the solutions that are closer to the global best solution reliant on the operation idea.

The effectual upgrade has been used at this phase to receive or remove the upgraded pelican position, which is demonstrated in Eq. (6).

$$X_i = \begin{cases} x_{i,}^{p_2}, & F_i^{p_2} < F_i; \\ X_i, & else, \end{cases} \tag{6}$$

Where $F_i^{p_2}$ specifies its goal function value reliant on phase 2 and $x_{i,}^{p_2}$ is the i^{th} pelican's novel grade.

Most of the members are upgraded reliant on over initial and second stages, the finest candidate solutions would be upgraded by trusting on the novel population grade and the objective function values. The algorithm travels to the next iteration, and the suggested POA is dependent upon Eqs. (3) to (6) are repeated till the whole implementation has been finished. Lastly, as the best solution for the problem and the finest solutions of the candidate formed during the iterative process was presented.

In EPOA, the opposition-based learning technique is combined into the POA which will be a prevalent method for increasing the efficiency of metaheuristics. The technique begins with a random population. Consequently, an accurate solution could be accomplished while the random main population takes the outcome same as the optimum solution. Optimization begins with an arbitrary values from the better performance or opposite place of the outcomes that increase the time for the optimization. The OBL algorithm provides an opposite place for the outcome from the main population:

$$X_i^{OBL}(0) = X_i(0)^{\max} + X_i(0)^{\min} - X(0) \tag{7}$$

In Eq. (7), $X_i^{OBL}(0)$ describes the opposite location of X_i, and $X_i(0)^{\max}$ and $X_i(0)^{\min}$ represent the variables of minimum and maximum boundaries, respectively.

The newest place provides valued opportunities with higher probabilities for achieving improved outcomes. While $X_i^{OBL}(0)$ is in the finest place then $X_i(0)$, it must be a sub-state, and $X_i^{OBL}(0)$ will be computed by the cost function.

The POA algorithm derives a fitness function (FF) for the accomplishment of increased classification effectiveness. This finds a positive integer to indicate the outstanding performance of the candidate solutions. The minimum of the classifier error rate must be measured as given in Eq. (8).

$$\begin{aligned} fitness(x_i) &= Classifier\ Error\ \ Rate(x_i) \\ &= \frac{No.of\ \ misclassified\ \ samples}{Total\ No.of\ samples} \cdot 100 \end{aligned} \tag{8}$$

3.4 Classification using FNN model

The FNN architecture can be utilized for automated identification and classification of BC. The architecture of FNN has five layer structure splitted into the FNN subnet [22]. The 5th layer of included the coupling effects of two links due to their coupling effects among joints.

Layer 1: Input layer of FNN. The four nodes with input range e_1, ec_1, e_2, and ec_2 variable theoretical domain within $[-6,6]$. The inputs of the node is:

$$f_1(i) = x_{ki} \tag{9}$$

Where$i = 1,2; k = 1,2.x_{ki}$ indicates the i^{th} input of k^{th} subnet, and $f_1(i)$ represents the output of k^{th} subnets at 1^{st} layer.

Layer 2: The fuzzification layer of FNN, the affiliation function generation layer. The input e_1, ec_1, e_2, and ec_2 are split into seven nodes, viz., seven fuzzy language sets namely PM (positive medium), NM (negative medium), NB (negative large), Z (zero), PS (positive small), PB (positive large), and NS (negative small). There exist thirty nodes. The gaussian function is utilized as association function, and centroid of the Gaussian function parallel to the seven fuzzy groups are 6, 4, 2, 0, -2, -4, and -6, with width 2.

$$f_2(i,j) = e^{-((f(i)-c_{ij})/b_{ij})^2}) \tag{10}$$

In which, $f_2(i,j)$ symbolizes the second layer output of k^{th} subnets. c_{ij} and b_{ij} are the centroid and width of j^{th} fuzzy set of i^{th} input parameters of the k^{th} subnets correspondingly.

Layer 3: inference layer: Here, multiplication is applied rather than taking small operations.

$$f_3(i,j) = f_2(1,i)f_2(1,j) \tag{11}$$

Where $i = 1,2,\ldots,7;\ \ j = 1,2,\ldots,7$. $f_3(i,j)$ indicates the output of 3rd layer of k^{th} subnets.

Layer 4: A weighted average model is used for defuzzifying.

$$u_k = f_4(i,j)\left(\sum_{i,j=1}^{7} f_3(i,j)w_{ij}^{(3)}\right)\sum_{i,j=1}^{7} f_3(i,j) \tag{12}$$

Now, $w_{ij}^{(3)}$ indicates the weight connecting coefficients between the 3rd and 4th layers of the k^{th} subnets.

Layer 5: The output layer of FNN. This represents the coupling relationships among the two joints of the manipulator.

$$y_k = f_5(i,j) = \sum_{i=1}^{2}(u_i w_{ki}^{(4)}) \tag{13}$$

Where $w_{ki}^{(4)}$ indicates the weight coefficients between the 4th and 5th layer, which reveals the coupling among the joints.

4 Result analysis

In this section, the performance validation of the BCD-EPOADFF technique is examined by employing the BreakHis database [23]. It includes two sub datasets namely 100X and 200X datasets as defined in Table 1. The dataset of 100X comprises 644 benign samples and 1437 malignant samples. In addition, the 200X dataset contains 623 benign samples and 1390 malignant samples.

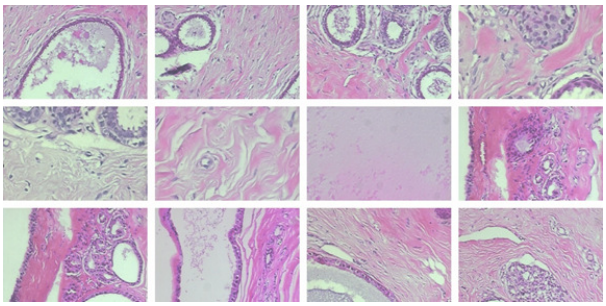

Fig. 3: Demonstrates the sample images.

Fig. 4 exhibits the confusion matrices generated by the BCD-EPOADFF system under the 100x dataset with 80:20 TRPH/TSPH and 70:30 TRPH/TSPH. These accomplished outcomes show the efficient recognition of the benign and malignant samples in every class.

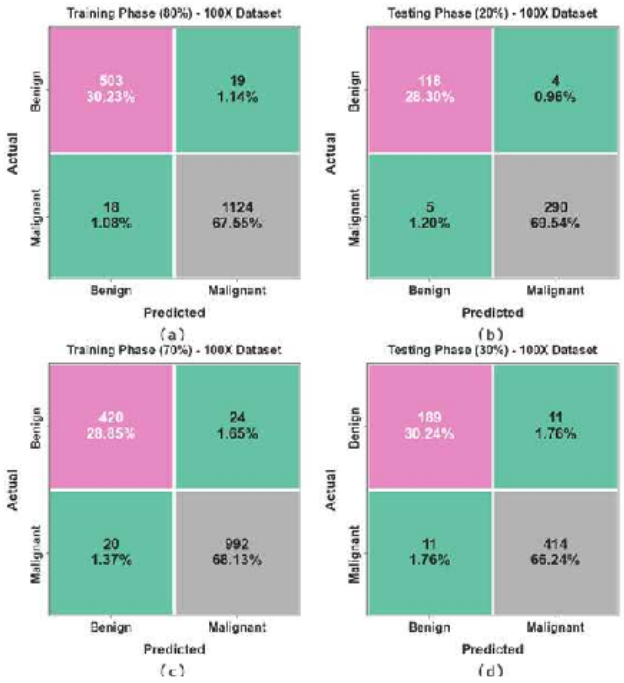

Fig. 4: Confusion matrices under the 100x dataset (a-b) 80:20 TRPH/TSPH and (c-d) 70:30 TRPH/TSPH

An overall classification analysis of the BCD-EPOADFF system with 100x dataset can be defined in Table 2 and Fig. 5. These obtained outcomes illustrate that the BCD-EPOADFF method gets successfully identification of benign and malignant classes. On 80% of TRPH, the BCD-EPOADFF technique gains average $accu_y$ of 97.78%, $sens_y$ of 97.39%, $spec_y$ of 97.39%, F_{score} of 97.42%, and MCC of 94.83%. Additionally, based on 20% of TSPH, the BCD-EPOADFF algorithm provides average $accu_y$ of 97.84%, $sens_y$ of 97.51%, $spec_y$ of 97.51%, F_{score} of 97.40%, and MCC of 94.80%. Meanwhile, with 70% of TRPH, the BCD-EPOADFF system gets an average $accu_y$ of 96.98%, $sens_y$ of 96.31%, $spec_y$ of 96.31%,F_{score} of 96.43%, and MCC of 92.86%. Finally, based on 30% of TSPH, the BCD-EPOADFF technique acquires average $accu_y$ of 96.48%, $sens_y$ of 95.96%, $spec_y$ of 95.96%, F_{score} of 95.96%, and MCC of 91.91%, respectively.

The $accu_y$ curves for training (TR) and validation (VL) exhibited in Fig. 6 for the BCD-EPOADFF algorithm with 100x dataset offer valued insights into its effectiveness with several epochs. Mainly, it can be a constant improvement at both TR and TS $accu_y$ with increased epochs that specifies the proficiency of the model for learnable and recognizable patterns from both data of TR and TS. The rising trends in TS $accu_y$

Table 1: Details on the dataset

	No. of Images	
Classes	100X	200X
Benign	644	623
Malignant	1437	1390
Total Images	2081	2013

Table 2: Overall classification results of the BCD-EPOADFF model under 100x dataset

Class	$accu_y$	$sens_y$	$spec_y$	F_{score}	MCC
TRPH (80%)					
Benign	97.78	96.36	98.42	96.45	94.83
Malignant	97.78	98.42	96.36	98.38	94.83
Average	97.78	97.39	97.39	97.42	94.83
TSPH (20%)					
Benign	97 .84	96.72	98.31	96.33	94.80
Malignant	97 .84	98.31	96.72	96.72	94.80
Average	97 .84	97.51	97.51	97.40	94.80
TRPH (70%)					
Benign	96.98	94.59	98.02	95.02	92.86
Malignant	96.98	98.02	94.59	97.83	92.86
Average	96.98	96.31	96.31	96.43	92.86
TSPH (30%)					
Benign	96.48	94.50	97.41	94.50	91.91
Malignant	96.48	97.41	94.50	97.41	91.91
Average	96.48	95.96	95.96	95.96	91.91

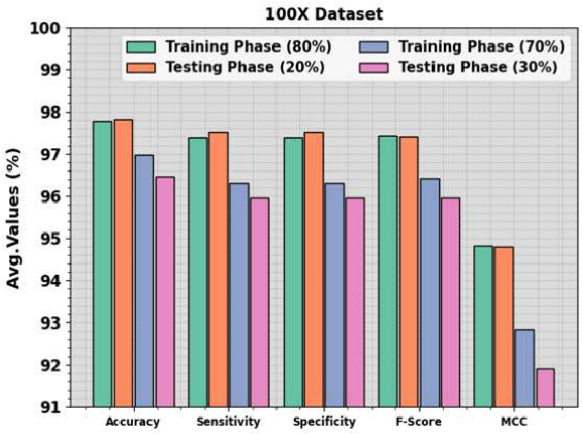

Fig. 5: Average of the BCD-EPOADFF system on 100x dataset

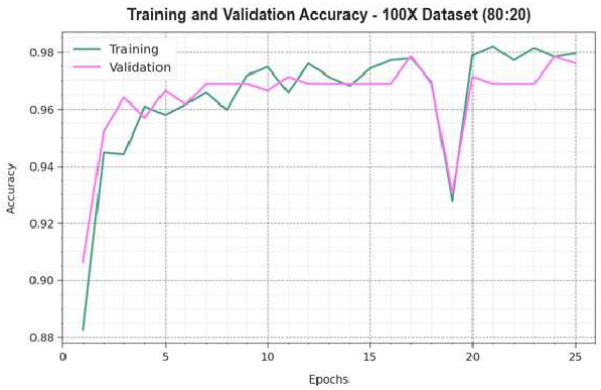

Fig. 6: $Accu_y$ curve of the BCD-EPOADFF technique under 100x dataset

underscore the adaptability to the TR dataset and the ability to produce correct predictions on unnoticed data, emphasizing capabilities of robust generalization.

Fig. 7 illustrates an extensive analysis of the TR and TS loss values for the BCD-EPOADFF system at 100x dataset in multiple epochs. This TR loss consistently minimizes as the model refines the weights to decrease classification errors. These loss curves represent the alignment of model with the TR data, underscoring the ability to capture patterns successfully. Significant can be the incessant enhancement of parameters in the BCD-EPOADFF algorithm, aimed to lesser differences between predictable and actual TR labels.

Fig. 7: Loss curve of the BCD-EPOADFF system under 100x dataset

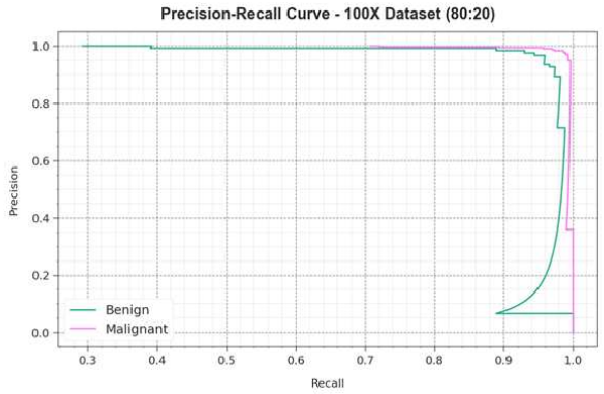

Fig. 8: PR curve of the BCD-EPOADFF model with 100x dataset

As regards the PR curve illustrated in Fig. 8, the findings affirm that the BCD-EPOADFF system with a 100x dataset constantly accomplishes enhanced PR values at every class. These results accentuate the model's efficient capacity for discrimination between diverse classes, underscoring its efficacy at exactly recognizing class labels.

Similarly, we show ROC curves generated by the BCD-EPOADFF algorithm with a 100x dataset in Fig. 9, indicating its proficiency in differentiating between classes. It provides respected insights into how the trade-off amongst FPR and TPR differs through various classification thresholds and epochs. These results emphasize the model's precise classification efficiency on diverse class labels, underscoring its effectiveness in overcoming several classification challenges.

Fig. 10 displays the confusion matrices accomplished by the BCD-EPOADFF system under 200x dataset at

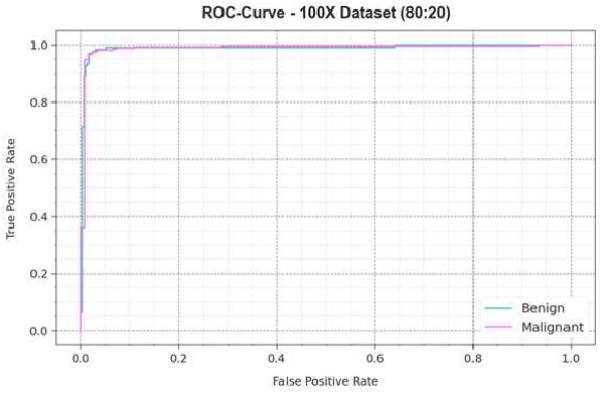

Fig. 9: ROC curve of the BCD-EPOADFF algorithm with 100x dataset

80:20 TRPH/TSPH and 70:30 TRPH/TSPH. These findings indicate the effective recognition of the benign and malignant samples with every class.

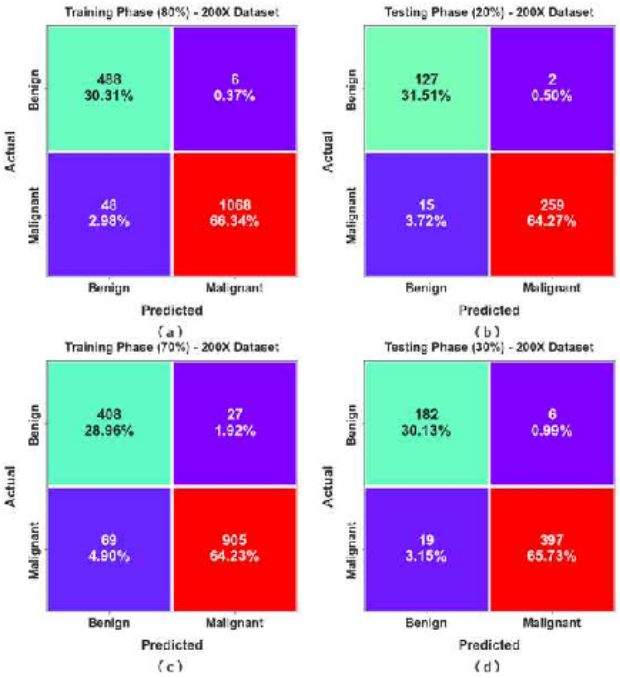

Fig. 10: Confusion matrices under the 200x dataset (a-b) 80:20 TRPH/TSPH and (c-d) 70:30 TRPH/TSPH

An overall classification analysis of the BCD-EPOADFF system under the 200x dataset can be determined in Table 3 and Fig. 11. These achieved outcomes demonstrate that the BCD-EPOADFF technique obtains efficient identification of benign and malignant categories. According to 80% of TRPH, the

BCD-EPOADFF algorithm gets average $accu_y$ of 97.24%, $sens_y$ of 97.24%, $spec_y$ of 97.24%, F_{score} of 96.15%, and MCC of 92.46%. Moreover, with 20% of TSPH, the BCD-EPOADFF method offers average $accu_y$ of 96.49%, $sens_y$ of 96.49%, $spec_y$ of 96.49%,F_{score} of 95.27%, and MCC of 90.80%. Similarly, based on 70% of TRPH, the BCD-EPOADFF technique acquires average $accu_y$ of 93.19%, $sens_y$ of 93.35%, spec_y of 93.35%, F_{score} of 92.22%, and MCC of 84.65%. Also, on 30% of TSPH, the BCD-EPOADFF algorithm gets an average $accu_y$ of 95.86%, $sens_y$ of 96.12%, $spec_y$ of 96.12%, F_{score} of 95.26%, and MCC of 90.64%, correspondingly.

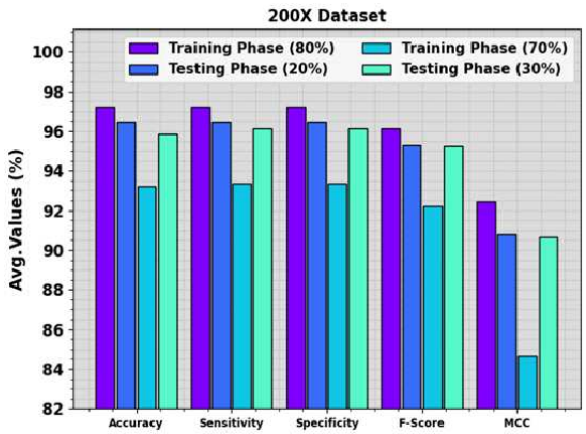

Fig. 11: Average of the BCD-EPOADFF model with 200x dataset

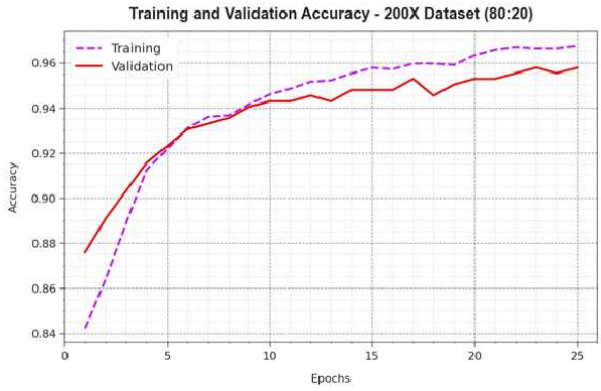

Fig. 12: $Accu_y$ curve of the BCD-EPOADFF technique with 200x dataset

The $accu_y$ curves for TR and VL illustrated in Fig. 12 for the BCD-EPOADFF system with 200x dataset provides valued insights into its efficiency in several epochs. Primarily, it can be a reliable upgrading at the TR and TS $accu_y$ with raised epochs, exhibiting the proficiencies of the model for learning and recognizing patterns from the data of TR and TS. The increasing trends in $TSaccu_y$ emphasize the flexibility model to the TR dataset and the ability to produce correct predictions on hidden data, underlining capabilities of robust generalization.

Fig. 13 represents a wide-ranging analysis of the TR and TS loss values for the BCD-EPOADFF technique with 200x dataset at multiple epochs. This TR loss constantly minimizes as a model refines the weights for decreasing classification errors. These loss curves explain the arrangement model with the TR data, accentuating the ability for capturing patterns successfully. Noteworthy can be the incessant improvement of parameters in the BCD-EPOADFF method, aimed at diminishing differences between actual and predictive TR labels.

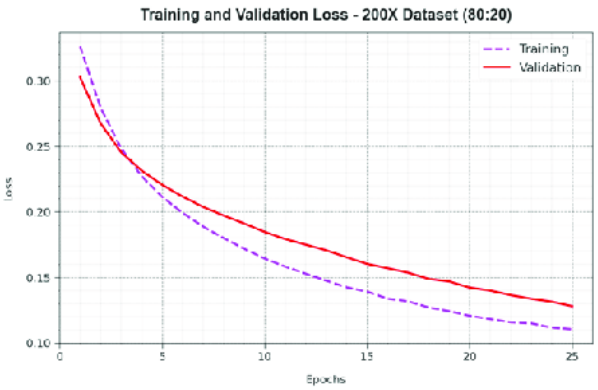

Fig. 13: Loss curve of the BCD-EPOADFF model with 200x dataset

As regards the PR curve illustrated in Fig. 14, the findings affirm that the BCD-EPOADFF system with a 200x dataset continually realizes superior PR values at every class. These results accentuate the efficient capacity of the model for discrimination between varied classes, underlining its effectiveness at precisely recognizing class labels.

Simultaneously, we display ROC curves generated by the BCD-EPOADFF algorithm with a 200x dataset in Fig. 15, specifying its proficiency in distinguishing between classes. These curves give value insights into how the trade-off between FPR and TPR differs through several classification epochs and thresholds. These results emphasize the precise classification efficiency of the model on diverse class labels, highlighting its effectiveness in overcoming multiple classification challenges.

Table 3: Overall classification analysis of the BCD-EPOADFF system under 200x dataset

Class	$accu_y$	$sens_y$	$spec_y$	F_{score}	MCC
TRPH (80%)					
Benign	98.79	98.79	95.70	94.76	92.46
Malignant	95.70	95.70	98.79	97.53	92.46
Average	97.24	97.39	97.39	96.15	92.46
TSPH (20%)					
Benign	98.45	98.45	94.53	93.73	90.80
Malignant	94.53	94.53	98.45	96.82	90.80
Average	96.49	96.49	96.49	95.27	90.80
TRPH (70%)					
Benign	93.19	93.79	92.92	89.47	84.65
Malignant	93.19	92.92	93.79	94.96	84.65
Average	93.19	93.35	93.35	92.22	84.65
TSPH (30%)					
Benign	95.86	96.81	95.43	93.57	90.64
Malignant	95.86	95.43	96.81	96.95	90.64
Average	95.86	96.12	96.12	95.26	90.64

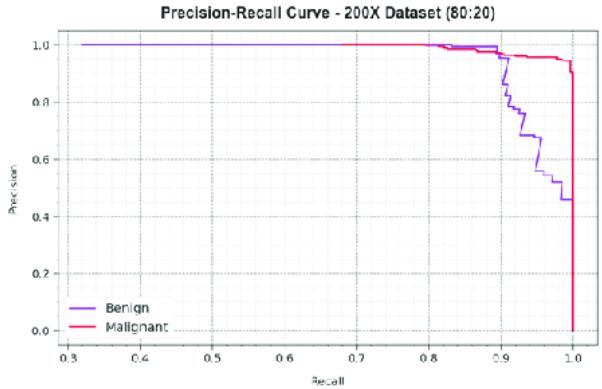

Fig. 14: PR curve of the BCD-EPOADFF method under 200x dataset

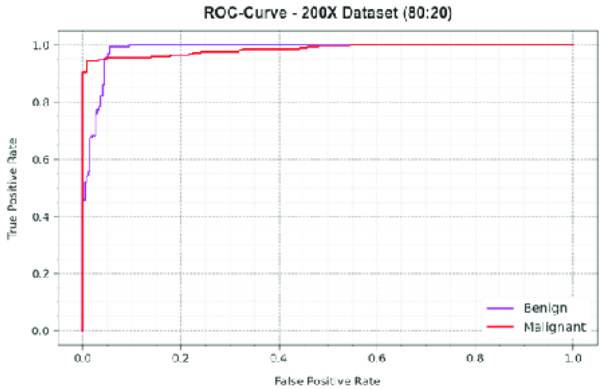

Fig. 15: ROC curve of the BCD-EPOADFF model on the 200x dataset

A brief comparative result of the BCD-EPOADFF technique with recent systems can be provided in Table 4 and Fig. 16 [11]. These accomplished findings indicate that the Incep. V3, VGG16, and ResNet-50 algorithms have obtained worse performance with least accu_y values of 81.67%, 80.15%, and 82.18%, respectively. At the same time, the DTLRO-HCBC, Incep. V3-LSTM, and Incep. V3-BiLSTM systems have shown closer accu_y values of 93.52%, 91.46%, and 92.05%, respectively. Though the AOADL-HBCC technique gains near optimal accu_y of 96.77%, the BCD-EPOADFF technique exhibits superior performance with a maximum accu_y of 97.84%. Therefore, the BCD-EPOADFF technique can be applied for enhanced classification performance.

5 Conclusion

In this article, we have developed an automated Histopathological Imaging Analysis for the BCD-EPOADFF technique. The purpose of the BCD-EPOADFF technique is to examine the HI for the detection and classification of BC. The BCD-EPOADFF algorithm comprises AMF-based preprocessing, feature fusion model, POA-based hyperparameter tuning, and FNN-based classification process. Initially, the AMF technique can be applied to get rid of the noise and enhance the image quality. In the BCD-EPOADFF technique, a deep feature fusion process takes place comprising three DL models namely ResNet, EfficientNet, and InceptionNet. Moreover, the hyperparameter tuning of the DL models takes place using EPOA which incorporates the traditional POA with the OBL concept. Finally, the FNN model can be

Table 4: Comparison outcome of the BCD-EPOADFF technique with other algorithms

Methods	Accuracy (%)
BCD-EPOADFF	97.84
AOADL-HBCC	96.77
DTLRO-HCBC	93.52
Incep.V3	81.67
Incep.V3-LSTM	91.46
Incep.V3-BiLSTM	92.05
VGG16	80.15
ResNet-50	82.18

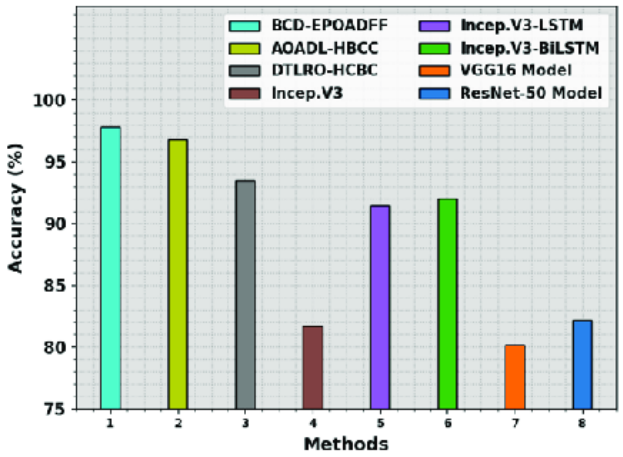

Fig. 16: Accu$_y$ analysis of the BCD-EPOADFF model compared with other systems

employed for automated detection and classification of BC. To validate the enriched performance of the BCD-EPOADFF method, a wide range of simulations were involved. The accomplished outcomes stated the superior performance of the BCD-EPOADFF method over other systems with respect to distinct measures.

Acknowledgment: The authors extend their appreciation to Umm Al-Qura University, Saudi Arabia, for funding this research work through grant number: 25UQU4310245GSSR03R.

Funding Statement: This research work was funded by Umm Al-Qura University, Saudi Arabia, under grant number 25UQU4310245GSSR03R.

References

[1] Huang, P.W., Ouyang, H., Hsu, B.Y., Chang, Y.R., Lin, Y.C., Chen, Y.A., Hsieh, Y.H., Fu, C.C., Li, C.F., Lin, C.H. and Lin, Y.Y., 2023. Deep-learning based breast cancer detection for cross-staining histopathology images. Heliyon, 9(2).

[2] Reshma, V.K., Arya, N., Ahmad, S.S., Wattar, I., Mekala, S., Joshi, S. and Krah, D., 2022. Detection of breast cancer using histopathological image classification dataset with deep learning techniques. BioMed Research International, 2022.

[3] Senan, E.M., Alsaade, F.W., Al-Mashhadani, M.I.A., Theyazn, H.H. and Al-Adhaileh, M.H., 2021. Classification of histopathological images for early detection of breast cancer using deep learning. Journal of Applied Science and Engineering, 24(3), pp.323-329.

[4] KIRELLİ, Y. and AYDIN, G., 2023. Classification of Histopathological Images in Automatic Detection of Breast Cancer with Deep Learning Approach. International Journal of Computational and Experimental Science and Engineering, 9(4), pp.359-367.

[5] Joseph, A.A., Abdullahi, M., Junaidu, S.B., Ibrahim, H.H. and Chiroma, H., 2022. Improved multi-classification of breast cancer histopathological images using handcrafted features and deep neural network (dense layer). Intelligent Systems with Applications, 14, p.200066.

[6] Toma, T.A., Biswas, S., Miah, M.S., Alibakhshikenari, M., Virdee, B.S., Fernando, S., Rahman, M.H., Ali, S.M., Arpanaei, F., Hossain, M.A. and Rahman, M.M., 2023. Breast cancer detection based on simplified deep learning technique with histopathological image using BreaKHis database. Radio Science, 58(11), pp.1-18.

[7] Verma, A., Panda, A., Kumar Chanchal, A., Lal, S. and Raghavendra, B.S., 2021. Automatic deep learning framework for breast cancer detection and classification from H&E stained breast histopathology images. Data Science: Theory, Algorithms, and Applications, pp.215-227.

[8] Nguyen, T.B.T., Ngo, M.V. and Nguyen, V.P., 2022, April. Histopathological imaging classification of breast tissue for cancer diagnosis support using deep learning models. In International Conference on Industrial Networks and Intelligent Systems (pp. 152-164). Cham: Springer International Publishing.

[9] Rajput, A., Yadav, M., Yadav, S., Chhabra, M. and Agarwal, A.P., 2023. Patch-Based Breast Cancer Histopathological Image Classification using Deep Learning. International Journal of Performability Engineering, 19(9), p.607.

[10] Sethy, P.K. and Behera, S.K., 2022. Automatic classification with concatenation of deep and handcrafted features of histological images for breast carcinoma diagnosis. Multimedia Tools and Applications, 81(7), pp.9631-9643.

[11] Obayya, M., Maashi, M.S., Nemri, N., Mohsen, H., Motwakel, A., Osman, A.E., Alneil, A.A. and Alsaid, M.I.,

2023. Hyperparameter optimizer with deep learning-based decision-support systems for histopathological breast cancer diagnosis. Cancers, 15(3), p.885.
[12] Hirra, I., Ahmad, M., Hussain, A., Ashraf, M.U., Saeed, I.A., Qadri, S.F., Alghamdi, A.M. and Alfakeeh, A.S., 2021. Breast cancer classification from histopathological images using patch-based deep learning modeling. IEEE Access, 9, pp.24273-24287.
[13] Chattopadhyay, S., Dey, A., Singh, P.K., Oliva, D., Cuevas, E. and Sarkar, R., 2022. MTRRE-Net: A deep learning model for detection of breast cancer from histopathological images. Computers in Biology and Medicine, 150, p.106155.
[14] Sampath, N. and Srinath, N.K., 2023. Breast cancer detection from histopathological image dataset using hybrid convolution neural network. International Journal of Modeling, Simulation, and Scientific Computing, p.2441003.
[15] Demir, F., 2021. DeepBreastNet: A novel and robust approach for automated breast cancer detection from histopathological images. Biocybernetics and biomedical engineering, 41(3), pp.1123-1139.
[16] Hameed, Z., Garcia-Zapirain, B., Aguirre, J.J. and Isaza-Ruget, M.A., 2022. Multiclass classification of breast cancer histopathology images using multilevel features of deep convolutional neural network. Scientific Reports, 12(1), p.15600.
[17] Su, Z., Niazi, M.K.K., Tavolara, T.E., Niu, S., Tozbikian, G.H., Wesolowski, R. and Gurcan, M.N., 2023. BCR-Net: A deep learning framework to predict breast cancer recurrence from histopathology images. Plos one, 18(4), p.e0283562.
[18] Yang, Y. and Guan, C., 2022. Classification of histopathological images of breast cancer using an improved convolutional neural network model. Journal of X-Ray Science and Technology, 30(1), pp.33-44.
[19] Ali, H.M., 2018. MRI medical image denoising by fundamental filters in "High-Resolution Neuroimaging-Basic Physical Principles and Clinical Applications". High-Resolution Neuroimaging, IntechOpen.
[20] LE DINH, T.U.A.N., 2023. COVID-19 Detection and Severity Grading with Chest-Xray and CT-Scan Using Deep Learning (Doctoral dissertation, Pukyong National University).
[21] Thota, S. and Menaka, D., 2024. Botnet detection in the internet-of-things networks using a convolutional neural network with the pelican optimization algorithm. Automatika, 65(1), pp.250-260.
[22] Shen, Y., 2024. Robotic trajectory tracking control system based on fuzzy neural network. Measurement: Sensors, p.101006.
[23] https://www.kaggle.com/datasets/ambarish/breakhis

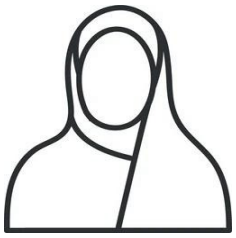

Arwa Alzughaibi is an Assistant Professor of Software Engineering at Taibah University. Her research interests include artificial intelligence, machine learning, deep learning, image processing, and digital transformation. She has published research papers in prestigious international journals in her areas of interest.

Maryam Alsolami is an Assistant Professor in the Department of Computer Science and Artificial Intelligence at Umm Al-Qura University in Makkah, Saudi Arabia. She holds a Ph.D. in Computer Science from Florida State University, a Masters' degree from DePaul University, and a Bachelor's degree from Umm Al-Qura University, all in Computer Science.

Mohammed Alshahrani is an Assistant Professor at Najran University, specializing in Artificial Intelligence, Natural Language Processing, and Data Science. I hold a Ph.D. in Computer Science from the University of Essex, UK. My research focuses on AI in general, NLP, machine learning, and big data analytics, with multiple publications in renowned journals.

Sultan Almalki is currently an Assistant Professor in the Computer Department at the Applied College, Najran University, Saudi Arabia. He received his B.Sc. degree in Information Systems from King Abdulaziz University, Saudi Arabia, his M.Sc. degree in Computer Science from Saint Xavier University, USA, and his Ph.D. degree in Computer Science from the University of Idaho, USA. His research interests include, but are not limited to, malware analysis, data analysis, intrusion detection systems (IDS), artificial intelligence, and machine learning.

Mohammed Al-Jabbar: is an Assistant Professor at Najran University, holding a Ph.D. in Computer Science. With expertise in educational technology, information retrieval (IR), artificial intelligence (AI), and natural language processing (NLP). Dr. Mohammed Al-Jabbar is dedicated to exploring the potential of advanced technologies to enhance the educational experience. His research focuses on integrating AI and NLP tools within educational environments, aiming to make learning more interactive, accessible, and engaging for students. At Najran University, Dr. Mohammed Al-Jabbar develops innovative educational solutions and immersive learning experiences that support diverse student needs and learning styles. His commitment to advancing educational technology reflects a vision of bridging cutting-edge research with effective, practical applications in the classroom. Through his work, Dr. Mohammed Al-Jabbar strives to contribute meaningfully to the field of educational technology, helping shape the future of digital learning and preparing students to thrive in a technology-driven world.

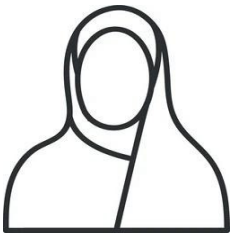

Randa Alharbi: Associate Professor with a distinguished career in academia and leadership roles. Accomplished in statistical research, data science, and e-learning. Actively contributing to academic and professional communities through various committees and associations.